HHS Public Access

Author manuscript

Neuroimage. Author manuscript; available in PMC 2022 August 15.

Published in final edited form as:

Neuroimage. 2022 August 15; 257: 119244. doi:10.1016/j.neuroimage.2022.119244.

Graph theory analysis identified two hubs that connect sensorimotor and cognitive and cortical and subcortical nociceptive networks in the non-human primate

Ruiqi Wu[a,b,e], **Feng Wang**[a,b], **Pai-Feng Yang**[a,b], **John C Gore**[a,b,d], **Li Min Chen**[a,b,c,*]

[a]Institute of Imaging Science, Vanderbilt University Medical Center, Nashville, TN 37232, United States

[b]Department of Radiology and Radiological Sciences, Institute of Imaging Science, Vanderbilt University Medical Center, 1161 21st Ave. S. AA 1105 MCN, Nashville, TN 37232-2310, United States

[c]Department of Psychology, Vanderbilt University, Nashville, TN 37232, United States

[d]Department of Biomedical Engineering, Vanderbilt University, Nashville, TN 37232, United States

[e]State Key Laboratory of Medical Neurobiology and MOE Frontiers Center for Brain Science, Institutes of Brain Science, Fudan University, Shanghai 200032, China

Abstract

Pain perception involves multiple brain regions and networks. Understanding how these brain networks work together is fundamental for appreciating network-wise changes reported in patients with chronic pain disorders. Parcellating pain related networks and understanding their causal relationships is the first step to understand how painful information is processed, integrated, and modulated, and it requires direct manipulation of specific brain regions. Nonhuman primates (NHP) offer an ideal model system to achieve these goals because cortical and subcortical regions in the NHP brain are established based on a variety of different types of data collected in a way that is not feasible or, at least, extremely difficult in humans (i.e., histology data, tract-tracing, intracerebral recordings). In addition, different methodological techniques can also

*Corresponding author at: Department of Radiology and Radiological Sciences, Institute of Imaging Science, Vanderbilt University Medical Center, 1161 21st Ave. S. AA 1105 MCN, Nashville, TN 37232-2310, United States. limin.chen@vanderbilt.edu (L.M. Chen).

Code and data availability statement

The data produced in the present study are available upon reasonable request to the corresponding author. The codes for fMRI data analysis and graph-theory analysis can be found in the AFNI (https://afni.nimh.nih.gov), the FSL (https://fsl.fmrib.ox.ac.uk/fsl/fslwiki), and the Brain Connectivity Toolbox (https://www.nitrc.org/projects/bct).

Declaration of Competing Interest

None.

Credit authorship contribution statement

Ruiqi Wu: Conceptualization, Investigation, Data curation, Formal analysis, Writing – original draft, Funding acquisition. **Feng Wang:** Investigation, Data curation. **Pai-Feng Yang:** Investigation, Formal analysis. **John C Gore:** Writing – review & editing, Funding acquisition. **Li Min Chen:** Conceptualization, Writing – original draft, Writing – review & editing, Funding acquisition.

Supplementary materials

Supplementary material associated with this article can be found, in the online version, at doi:10.1016/j.neuroimage.2022.119244.

help characterize and further understand these brain cortical and subcortical regions over the course of development. Here we used a heat nociceptive stimulation that is proven to elicit activity of nociceptive neurons in the cortex to refine and parcellate the whole brain nociceptive functional networks, to identify key network hubs, and to characterize network-wise temporal dynamic signatures using high-resolution fMRI. We first functionally localized 24 cortical and subcortical regions that responded to heat nociceptive stimuli (somatosensory area 1/2, area 3a/3b, S2, posterior insula (pIns), anterior insula, area 7b, posterior parietal cortex, anterior cingulate cortex (ACC), prefrontal cortex, caudate, and mediodorsal (MD) and ventral posterior lateral (VPL) thalamic nuclei) and used them as seeds in resting state fMRI (rsfMRI) data analysis. We applied both hierarchical clustering and graph-theory analyses of the pairwise rsfMRI correlation metrics and identified five cortical and one subcortical sub-networks: strong resting state functional connectivity (rsFC) between ACC and prefrontal regions, parietal cortex and area 7b, S2 and posterior insula, areas 3a/3b and 1/2 within the S1 cortex, and thalamic MD and caudate nuclei. The rsFC strengths between cortical areas within each subnetwork were significantly stronger than those between subcortical regions. Regions within each sub-network also exhibited highly correlated temporal dynamics at rest, but the overall dynamic patterns varied drastically across sub-networks. Graph-theory analysis identified the MD nucleus as a hub that connects subcortical and cortical nociceptive sub-networks. The S2-pIns connection joins the sensory and affective/cognitive sub-networks.

Keywords

Resting-state functional connectivity; Graph theory; Whole brain; Pain; Non-human primate; Brain network

1. Introduction

Advances in functional imaging techniques, including fMRI, MEG and EEG, have allowed direct visualization and examination of supraspinal mechanisms associated with acute pain perception and chronic pain, and have identified engagement of widespread brain regions and multiple networks (e.g., sensorimotor, affective, cognitive as well as emotional), for reviews see Apkarian et al. (2013, 2005), Kucyi and Davis (2015, 2017). FMRI activation patterns, termed heat pain signature, predict the subjective perception of heat pain in normal subjects (Wager et al., 2013). Because many (if not all) of these brain regions involved multiple brain functions, one remaining critical question is how these different regions and networks causally interconnect and integrate painful information. To answer this question, it is essential to be able to directly perturb (stimulate, inhibit or shut down) activity at specific nociceptive processing brain regions while monitoring the changes in the networks. Ethical and technical concerns constrain such studies in humans. Nonhuman primates (NHP) provide alternative models for such studies aiming to dissect networks and identify key hubs because cortical and subcortical regions are determined by multifaced features such as cytoarchitectonic features, anatomical connections, and neuronal activity properties. In animal models, invasive recording and stimulation methods can be combined and used to achieve high precision network perturbation (Gerits et al., 2012; Klink et al., 2021; Xu et al., 2019; Yang et al., 2021). Supporting this notion, our previous work in NHPs

demonstrated that many core brain regions involved in human pain perception remained active during processing of heat nociceptive stimulation under light anesthesia (Wu et al., 2017). Moreover, refined subnetworks are not readily distinguishable in the human brain, likely due to the low resolution of human fMRI studies, the proximity between regions, and lack of detailed anatomically validated atlas. For example, at the lateral sulcus region (the equivalent of the Sylvian fissure in the human brain), multiple areas reside (e.g., S2, posterior insula (pIns), and area 7b) in close proximity that are believed to represent the nature and/or magnitude of pain sensation (Isnard et al., 2011; Kim et al., 2017; Segerdahl et al., 2015) and have shown robust nociceptive heat stimulation related fMRI responses. S2 and posterior insula are not readily distinguishable in the human brain (Sawamoto et al., 2000). Moreover, we have identified sub-modality (cold, heat, and mechanical) nociceptive responsive regions that are organized as separated patches and in distinct patterns (Chen et al., 2011, 2012; Wu et al., 2017; Yang et al., 2018). These meso-scale patch-like organizations have not been reported in the human brain. This patch-like organization is functionally relevant because our subsequent intracranial electrophysiology mapping and recordings identified clustered nociceptive heat neurons at one S2 region that showed robust fMRI signal changes to nociceptive heat stimulation (Ye et al., 2021). To date, to our knowledge, this is the first line of evidence supporting that fMRI signal changes indeed reflect the neural activity of nociceptive neurons (Chen et al., 2011; Yang et al., 2018; Ye et al., 2021) at a millimeter scale. Using these functionally identified S2 and pIns as seed regions, we found that these two key regions connect to two non-overlapping cortical networks (Wu et al., 2017). These resting-state functional connectivity (rsFC) networks are surrogates of intrinsic nociceptive networks because rsFC measured with resting state fMRI (rsfMRI) signals reflects neuronal functional connectivity (Chen et al., 2017; Wang et al., 2013; Wilson et al., 2016), for a review see Chen et al. (2017).

Building upon our and others' previous work, here we aimed to map and delineate cortical and subcortical nociceptive sub-networks at the whole brain level by applying both seed-based and data-driven clustering and graph theory analysis of rsfMRI signals. We also explored whether the temporal dynamics have a signature feature of each network and characterize the networks' temporal dynamic features. Specifically, we addressed the following questions: what is the hierarchical functional organization of brain regions that are involved in nociceptive information processing? How are nociceptive sub-networks interconnected and through which hubs? Does each sub-network exhibit its own distinct dynamic functional connectivity features? The findings derived from the present study will help to establish the fundamental network organization principles of the primate pain system, and, therefore, could also inform the construction of pain-specific mathematical network models for guiding rsFC analysis in human pain fMRI studies. Moreover, identification of key hubs will guide future direct stimulation studies that aim to dissect the whole brain pain circuits and understand the causal connections and information processing flow in the primate brain. By combining heat nociceptive stimulation and resting-state fMRI, we identified six nociceptive sub-networks and hubs interconnecting them.

2. Methods and materials

2.1. Animal preparation

Three adult male squirrel monkeys (*Saimiri sciureus*) (SM-H, SM-G, and SM-S) were studied. Data from four imaging sessions were included in the quantification (one animal underwent two sessions). For the fMRI experiments, animals were initially sedated with ketamine hydrochloride (10 mg/kg, im) and given atropine sulfate (0.05 mg/kg, im), and then anesthetized with isoflurane (0.7%–1.2%) delivered in a 70:30 N_2O/O_2 mixture. After intubation, the animal was placed in a custom-designed MR cradle with the head secured in a plastic stereotaxic frame with two plastic ear bars and one head bar. During fMRI data acquisition, animals were maintained at a light (0.7–0.9% isoflurane) and stable level of anesthesia. 2.5% dextrose in saline solution was infused intravenously (3 ml/kg/h) to prevent dehydration. Animals were artificially ventilated to maintain an end-tidal CO_2 of 4%. Rectal temperature was maintained (SA Instruments) between 37.5 °C and 38.5 °C using a circulating water blanket. Heart rate (EKG, SA instruments), peripheral capillary oxygen saturation (SpO_2; Nonin), respiration pattern, and end-tidal CO_2 (22–26 mmHg; SurgiVet) were continuously monitored during the entire procedure. During fMRI data acquisition, the heart rate was stable, with changes of $\langle$ 10 bpm during stimulation. SpO_2 was also stable, remaining at $\rangle$ 95% during the entire experiment. All procedures were conducted by following National Institutes of Health and ARRIVE guidelines and were approved by the Institutional Animal Care and Use Committee of Vanderbilt University.

2.2. Stimulation protocol

The subjects' fingers were stabilized with modeling clay, palm side up, leaving the glabrous skin of the distal finger pads available for stimulation. Noxious heat (47.5 °C) stimuli were presented on the distal and middle phalanges of D2 and D3 of the dominant hand simultaneously (right hands in all monkeys) via a CHEPS thermal probe with a rapid heating rate of 70 °C/s (Medoc Advanced Medical Systems). For a typical fMRI noxious heat (47.5 °C) stimulation run, 21 s duration blocks of 47.5 °C heat were repeated nine times with a 30 s baseline (32 °C) period in between.

2.3. MRI data acquisition and analyses

All MRI scans were performed on a 9.4 T 21 cm narrow-bore MRI scanner (Varian Medical Systems) using a quadrature birdcage volume coil (inner diameter = 85 mm, Doty 85) centered over the brain. A series of T2-weighted multi-slice gradient echo high-resolution structural axial images (TE = 10 ms, TR = 500 ms, 0.125 × 0.125 × 1 mm^3 voxel size, 512 × 512 × 28 matrix) were collected. FMRI data were acquired from the same slices using a two-shot gradient echo planar imaging (GE-EPI) sequence (TE = 16 ms, TR = 1.5 s, 1 × 1 × 1 mm^3 voxel size, 64 × 64 × 28 matrix, 3 s/volume, interleaved slices, linear K space filling). An extra navigator echo was collected with no phase encoding before the acquisition of the actual image data. This echo is used to correct for phase variations typically caused by motion. FMRI data with and without heat stimulation were collected with the same functional imaging acquisition parameters. In a typical fMRI session (day), 3–4 resting-state runs (170 vol per run) were acquired prior to stimulation runs. A total of four imaging sessions were performed (one monkey underwent two imaging sessions). Specifically, 12, 5,

8, and 9 stimulation runs and 4, 3, 4, and 3 rsfMRI runs were acquired from monkey SM-H (sessions 1 and 2), SM-G, and SM-S, respectively. Detailed data sampling information is provided in Supplementary Table 1.

Functional EPI data (stimulus and resting-state) were pre-processed with slice timing and head motion correction (3dTshift, AFNI_21.3.17), and physiological noise correction using a RETROICOR algorithm (3dretroicor, AFNI_21.3.17) (Glover et al., 2000). For image quality control, datasets with motion artifacts of head rotation > 0.3° or/and head translation > 0.2 mm (1/5 voxel size) were excluded from the subsequent analyses and quantification. To preserve the highest resolution possible, no spatial smoothing was applied. Stimulus-evoked EPI data were temporally high and low pass filtered in between 0.008 Hz and 0.25 Hz. High-pass filter was applied for de-trending the stimulus-evoked EPI data. RsfMRI data were filtered in between 0.01 Hz and 0.1 Hz (3dBandpass, AFNI_21.3.17). Activation maps were created by voxel-wise analysis, using the hemodynamic response function (HRF) convolved with the stimulus presentation paradigm (21 s stimulus on and 30 s stimulus off) (3dDeconvolve, AFNI_21.3.17). The HRF we used was the SPM gamma variate basis function, peaking at 12 s after event onset. Activation maps (FDR corrected, $p < 0.05$) were generated for each run. Multi-run activation maps were then created by a t-test performed on the β value of each run across multiple runs obtained within the same imaging session, and then displayed as statistical t-value maps (with a threshold of t-value = 2.5, $p < 0.05$, illustrated in Figs. 1 and 2). EPI data were up-sampled from 64 × 64 × 28 to 128 × 128 × 28 matrix size with linear interpolation (FLIRT, FSL), and co-registered on corresponding T2-weighted high-resolution anatomical images using a linear image registration tool (FLIRT, FSL) for display.

A seed-based rsfMRI analysis was performed to characterize the functional connectivity pattern and determine the intrinsic circuits of main nociceptive regions in each animal. Identification of seeds is critical for rsfMRI analysis. Because of the known functional heterogeneity within each anatomically defined region, we used both anatomical and functional criteria in selecting seed voxels. The anatomical location of each seed was determined by overlaying the multi-run heat-evoked activation map obtained in each imaging session on their corresponding three T2 weighted structural image planes (sagittal, axial, and coronal), and then on the squirrel monkey atlas, publications involving histology of squirrel monkeys (Gergen and MacLean, 1962; Jones and Burton, 1976) and an online reference (http://neurosciencelibrary.org/specimens/primates/squirrelmonk/). The selected seeds were based upon local maxima (i.e., several adjacent voxels showing robust responses to nociceptive stimuli) within each of the anatomically defined regions. Whole brain voxel-wise correlation map was generated (3dfim+, AFNI_21.3.17) by using filtered rsfMRI signals extracted from seeds (the strongest response cluster within each region of interest, ROI) as the predictors for each run. Multiple-run averaged correlation coefficient maps of S2 or VPL seeds were displayed (threshold r-value > 0.2, $p < 0.05$) with warmest color indicating the highest correlation value (e.g., Figs. 1B and 2B). 24 most consistently activated regions (in 60% of runs and subjects) during heat stimulation were selected as ROIs in the pair-wise resting-state connectivity analysis. Pair-wise correlation coefficients were then quantified across imaging sessions (days) and subjects. For illustration purposes, axial image slices with significant cortical activation and correlation foci, and three

reconstructed image planes (sagittal, axial, and coronal) with significant subcortical activation and correlation foci were displayed. The hemisphere on the same side as the stimulation was defined as the ipsilateral hemisphere, while the opposite was labeled as the contralateral one.

2.4. Inter-regional correlation and hierarchical cluster analysis

To investigate the relationship between these nociceptive regions, inter-regional correlations were then calculated. Twenty-four ROIs (ipsilateral and contralateral ACC (iACC, cACC), prefrontal cortex (iPF, cPF), area 7b (i7b, c7b), parietal cortex (iPari, cPari), posterior insula (ipIns, cpIns), S2 (iS2, cS2), anterior insula (iaIns, caIns), area 1/2 of S1 (i1/2, c1/2), area 3a/3b of S1 (i3a/3b, c3a/3b), ventral posterolateral (VPL) nucleus (iVPL, cVPL), mediodorsal (MD) thalamic nucleus (iMD, cMD), and caudate (iCau, cCau)) that showed activation to nociceptive heat stimuli were chosen for inter-regional correlation coefficient analysis. Specifically, Pearson correlations among these twenty-four main regions were calculated. 24 × 24 region-region correlation matrixes were generated using the correlation coefficient value (r value indicates the strength of rsFC) of averaged time-courses of each specific region pair. Each correlation coefficient was transformed using Fisher's Z, and then mean z-values were back transformed to the correlation coefficient (Gorsuch and Lehmann, 2010). Averaged inter-regional correlation coefficients (r-values) were calculated across all of the 14 rsfMRI runs from 3 animals and 4 sessions and are presented as matrix plots in Fig. 3A.

We then investigated the hierarchical relationship among all 24 regions by using a hierarchical clustering method (Edelbrock and McLaughlin, 1980; Johnson, 1967). Clustering was based on time courses of different regions and was determined using the correlation metric and weighted average linkage (WPGMA) clustering criterion (Sokal and Michener, 1958). The distance between clusters was calculated as a simple average. Hierarchical binary cluster trees were created (linkage, Matlab_R2020b), and then dendrogram plots of the cluster trees were generated (dendrogram, Matlab_R2020b) among these regions (Fig. 3B). On the tree graph, the length of each U-shaped line represents the distance between the connected regions.

2.5. Dynamic functional connectivity quantification

To further explore the temporal dynamic relationships between nociceptive regions, as well as sub-networks parsed by hierarchical cluster analysis, we quantified dynamic functional connectivity (DFC) using the sliding window correlation method (Hutchison et al., 2013a, 2013b; Shi et al., 2016; Wang et al., 2017). We computed windowed correlations between each of the two regions from the same sub-network by using sliding-window sizes of 60 s, 120 s, and 180 s. The selection of these three windows was based on our previous analysis (Shi et al., 2016). The scheme of DFC analysis across sub-networks is illustrated in Fig. 4A. One example of a dynamic correlation profile of all six sub-networks is displayed in Fig. 4A (right). To further quantify the relationship among fluctuation features of all of the sub-networks, Pearson correlations were calculated on two time-courses of windowed correlations (DFC pair) between any two regions within each sub-network and between any

two sub-networks. A p-value < 0.05 is considered as statistically significant, and results are expressed as mean ± standard error.

2.6. Graph theory analysis

We next performed data-driven graph-theory analysis to delineate pain sub-networks and to identify hubs that connect sub-networks. A common and useful representation of a network is the adjacency matrix (or connection matrix), which completely defines the topology of the network and is a common representation of a network defined by graph theory analysis (Fornito et al., 2010; Lv et al., 2016). The 24 × 24 inter-regional correlation matrix was converted to weighted undirected adjacency matrixes by applying a different threshold. The choice of the threshold was based upon the value of significant correlations ($r = 0.15$, $p < 0.05$; $r = 0.20$, $p < 0.01$; $r = 0.25$, $p < 0.005$; and $r = 0.27$ $p < 0.001$). All correlations above the given threshold are considered to be links (edges) between connecting nodes (vertex). The adjacency matrix element $a(i, j)$ is nonzero (above threshold) if there is a link between nodes i and j. Weighted undirected graphs (plotted in Pajek 5.14, University of Ljubljana, http://mrvar.fdv.uni-lj.si/pajek/, Batagelj and Mrvar, 1998) by assigning links to all supra-threshold correlations, converted from the averaged region-region correlation matrix, are illustrated in Fig. 5A (with the threshold of 0.16), Fig. 5B (with the threshold of 0.21), and Fig. 5F (with the threshold of 0.27). Dots represent nodes, lines connecting the dots indicate links, and line thickness indicates weights of the links (node strength). The number of links in a node is the degree of this node. Node strength and degree were calculated on adjacency matrixes from all 14 runs at four thresholds ($r = 0.15$, $r = 0.20$, $r = 0.25$, and $r = 0.27$) by using the Brain Connectivity Toolbox (Rubinov and Sporns, 2010). The strength and degree measures of the same region from both hemispheres were summed and averaged across runs. We pooled each region from both hemispheres when computing the node strength and degree because high functional connectivity (Fig. 3) and high similarity in rsFC maps (sFig. 1C) were observed between left and right hemisphere counterparts. Furthermore, 15 (i.e., C_6^2; 6 sub-networks in total) broken-down graphs based on any two subnetworks were illustrated to decompose the overall adjacency matrix. Connector hubs between any two sub-networks were parsed by comparing node degrees and strengths. The nodes with the highest degree in each sub-graph were considered to be potential hubs (if there was only one highest degree node, it was identified as a hub). Then, strengths were compared among the potential hubs, and the strongest one was determined to be a hub.

3. Results

The overall goal is to characterize the whole brain heat nociceptive networks and identify sub-networks using resting state fMRI signals. Figs. 1 and 2 illustrate how we use heat stimulation activation maps to functionally localize the cortical and subcortical ROIs for subsequent network analysis. Figs. 3 and 4 show sub-networks identified with a clustering method and their dynamic connectivity feature. Fig. 5 represents networks parcellated with graph theory analysis, and Fig. 6 summarizes the sub-network connection feature we identified with rsfMRI.

3.1. Similar heat activation and S2 rsFC maps

First, we mapped nociceptive heat-evoked activation at the whole brain scale. Similar to the observations in human fMRI studies (but in a much more refined regional manner), we detected heat nociceptive stimuli-evoked fMRI activation in widespread cortical and subcortical regions, including bilateral cortical area 7b (slice 1 in Fig. 1A), ACC (slice 3 in Fig. 1A), PF (slice 4 in Fig. 1A), Pari (slice 5 in Fig. 1A), area 3a/3b (slices 5 and 6 in Fig. 1A), S2 (slice 7 in Fig. 1A), pIns (slice 9 in Fig. 1A), area 1/2 (slice 10 in Fig. 1A), and aIns (slice 11 in Fig. 1A). Additionally, several subcortical regions, including caudate (purple circle in Fig. 2A1 and A2), MD (blue circle in Fig. 2A1 and A3), and VPL (red circle in Fig. 2A1 and A3), were also activated by nociceptive heat stimuli.

Brain-wise functional connectivity maps of the S2 seed (outlined by black line in slice 9 of Fig. 1A–C) exhibited very similar connectivity patterns (Fig. 1B) to the stimulus-evoked activation map (compare Fig. 1A with B). Bilateral area 7b (slice 1 in Fig. 1B), ACC (slice 3 in Fig. 1B), PF (slice 4 in Fig. 1B), area 3a/3b (slice 4 in Fig. 1B), Pari (slice 5 in Fig. 1A), pIns (slice 9 in Fig. 1B), area 1/2 (slice 10 in Fig. 1B), aIns (slice 11 in Fig. 1B), and contralateral S2 (slice 9 in Fig. 1B) were all strongly connected to the S2 seed. We noted that most of the activation (Fig. 1A) and correlation foci (Fig. 1B) were located uniformly on both hemispheres. Overlap maps (brown foci in Fig. 1C) of cortical activation (green foci in Fig. 1C) and rsFC of S2 seed (red foci in Fig. 1C) showed, overall, a high degree of spatial correspondence between these two maps. Across the entire brain, various degrees of spatial overlap were observed between nociceptive responsive (activation) and S2-connected (rsFC) regions. To reveal functional connectivity networks of subcortical regions, seeds were placed at the ipsilateral thalamic VPL nucleus (indicated in Fig. 2B1) and ipsilateral MD nucleus (indicated in Fig. 2B2) respectively. Fig. 2B illustrates the whole brain rsFC pattern. The reconstructed coronal image plane showed that bilateral MD and contralateral VPL had connections to the VPL seed (right in Fig. 2B1), and bilateral VPL and contralateral MD had connections to the MD seed (right in Fig. 2B2). The reconstructed sagittal image plane showed subcortical regions of MD, VPL, and caudate were inter-connected (middle in Fig. 2B1 and B2). The rsFC pattern was similar to the heat-evoked activation pattern in subcortical regions. However, the heat-evoked activations appeared to be more lateralized. The seed regions of the contralateral hemisphere might be more engaged in processing unilateral heat stimulation (comparing the middle panels in Fig. 2B with Fig. 2A1). Similar rsFC maps were observed when bilateral regions were used as seeds, respectively. RsFC maps for contralateral S2 and VPL are shown in Supplementary Figs. S1 and S3. Moreover, high commonalities were observed in the rsFC correlations between different somatosensory cortical seeds (contralateral and ipsilateral area 3a/3b and area 1/2) (Fig. S2). The similarity of the whole brain pattens qualitatively varied across animals. A second case and a few more representative ROI seeds are shown in supplementary Figs. S1–S3. It is worth noting that the significant clusters in the ipsilateral S2 and pIns were observed in VPL- and MD-seed based correlation maps (right in Fig. 2B1 and B2). It was indicated that thalamus could connect the cortical and subcortical regions.

3.2. Hierarchical organization of regions within rsFC sub-networks

To determine whether and to what extent nociceptive regions belong to different functional cortical sub-networks, we performed pair-wise inter-regional rsFC and hierarchical cluster tree analyses between all possible pairs of the brain regions (ROIs) that exhibited strong fMRI responses to nociceptive-heat stimuli, including bilateral S2, pIns and aIns, area 1/2, area 3a/3b, area 7b, bilateral Pari cortex, ACC, PF, VPL and MD thalamic nuclei, and Cau. The 24 × 24 matrix plot of the group averaged inter-regional correlation coefficients (*r*-values) showed a fixed pattern of strong rsFC among subgroups of regions (see each group outlined by dotted lines in Fig. 3A) and revealed that brain regions involved in processing nociceptive inputs are also highly inter-connected at rest. Three main clusters, having the strongest connections within a subgroup, were identified within the matrix. The strongest connections were observed between bilateral PF and ACC (orange-yellow patches between iPF-cPF, iACC-cACC in Fig. 3A). The second strongest connections were found between bilateral 7b and Pari (yellow-green patch between i7b-c7b, iPair-cPari, i7b-iPari, c7b-cPari, i7b-cPari, c7b-iPari in Fig. 3A). The third strongest connections were identified between pIns and S2 regions in the same hemisphere (blue-green patch between ipIns-iS2, and between cpIns-cS2 in Fig. 3A). Moreover, S2 was strongly connected with area 1/2 and area 3a/3b, which are outside of its subgroup. Bilateral subcortical regions (VPL, MD, and Cau) also exhibited robust connectivity among them (blue-green patches in Fig. 3A).

For hierarchical cluster tree analysis, the WPGMA distance measure was derived to rank the strength of inter-regional rsFC. The dendrogram plots of all twenty-four regions (Fig. 3B) showed that the distance between bilateral ACC and bilateral PF was the shortest, and between bilateral Pari cortex was the second shortest. The distances between bilateral 7b, bilateral S1 sub-regions (areas 3a/3b, 1/2), bilateral Cau, ipsilateral S2 and pins, or contralateral S2 and pIns were comparable and the third shortest. Distances between bilateral aIns and between bilateral thalamus regions were relatively larger. The longest distance was observed between bilateral VPL nuclei. According to the linkage distance in the hierarchical cluster tree, six clusters were identified (see the dotted colored lines in Fig. 3B): ACC-PF cluster (sub-network 1), 7b-Pari cluster (sub-network 2), S2-pIns cluster (sub-network 3), bilateral aIns cluster (sub-network 4), and areas l/2–3a/3b cluster (sub-network 5). Three subcortical regions (bilateral VPL, MD and Cau) were also clustered into a separate sub-network 6. Together, six separate and hierarchically organized nociceptive rsFC sub-networks were parsed.

3.3. Dynamic functional connectivity features of nociceptive sub-networks at rest

To explore the temporal dynamic connectivity features of pain regions within and across subnetworks, we calculated the temporal correlation between any two regions within the same sub-network or across sub-networks (Fig. 4). We found that regions within each sub-network exhibited highly synchronized temporal fluctuations (Fig. 4A). Interestingly, the degree of synchronization varied across sub-networks. Brain regions within each of the networks showed very similar temporal dynamic patterns (see red stripes in the right column in Fig. 4A). Across sub-networks, however, the temporal correlation dynamics varied. Regions within subcortical network 6 exhibited less synchronized fluctuation. Overall, the DFC between cortical regions was higher than that between subcortical regions (compare the

top 25 rows with the bottom 15 rows in DFC patterns in Fig. 4A and B). The same DFC patterns were retained in the sliding-window analysis using sliding windows of 60 s (right in Fig. 4A and upper in Fig. 4B), 120 s (middle in Fig. 4B), and 180 s (bottom in Fig. 4A).

To quantify the degree of DFC differences between sub-networks, we calculated the Pearson correlation between any two time-courses of DFC within and across any two sub-networks. The total number of DFC pairs is 210 for sub-network 1, 2, 3, or 5 (i.e., $C_6^2 \times 14$ runs) and 1470 (i.e., $C_{15}^2 \times 14$ runs) for sub-network 6. The total number of DFC pairs is 504 (i.e., $C_6^1 \times C_6^1 \times 14$ runs) for across sub-network pairs 1 & 2, 1 & 3, 1 & 5, 2 & 3, 2 & 5, or 3 & 5; 84 for across sub-network 1 & 4, 2 & 4, 3 & 4, or 4 & 5 (i.e., $C_6^1 \times C_1^1 \times 14$ runs); 1260 for across sub-network 1 & 6, 2 & 6, 3 & 6, or 5 & 6 (i.e., $C_6^1 \times C_{15}^1 \times 14$ runs); and 210 for across sub-network 4 & 6 (i.e., $C_1^1 \times C_{15}^1 \times 14$ runs). Regardless of the specific sliding-window used (60, 120 or 180 s), the regions within each sub-network exhibited highly correlated temporal dynamics at rest (see columns within the yellow shaded region in Fig. 4C1–C4). In contrast, correlations between regions across sub-networks were very low (see columns within the pink shading in Fig. 4C1–C4). Statistical analysis showed that the temporal correlations within the sub-network were higher than those across any two sub-networks (comparing yellow columns with pink columns in Fig. 4C1–C4). Many of these differences are statistically significant (Sidak's multiple comparisons tests, $p<0.05$). Generally, the temporal correlations between regions within cortical sub-networks were significantly higher than those between regions within the subcortical network (comparing sub-networks 1, 2, 3, and 5 with sub-network 6 in Fig. 4C2–C4). We also found weak temporal correlations across sub-networks 2 & 3, 2 & 4, 3 & 5, 3 & 6, and 5 & 6, and negative temporal correlations across sub-networks 1 & 6, 2 & 6, and 3 & 4. There was no significant difference between results at different sliding windows of 60 s (red columns in Fig. 4C1), 120 s (blue columns in Fig. 4C1), and 180 s (green columns in Fig. 4C1), except the difference between sliding windows of 60 s and 120 s for sub-network 2.

3.4. Graph theory analysis of nociceptive sub-networks

Graph theory analysis was applied to resting-state signals of the nociceptive regions within cortical and subcortical pain networks. We thresholded the networks at different r values to illustrate the overall connectivity patterns and their relative strengths (Fig. 5). The graph at the threshold of $r = 0.15$ (Fig. 5A) illustrates a quite complicated inter-regional network. However, links between cortical and subcortical regions were generally weaker, only were found between cACC & iMD, and ipIns & iMD. Upon increasing the threshold to $r = 0.20$ (Fig. 5B), the network was simplified after weak connections were excluded. Node degree (top in Fig. 5C) and strength (bottom in Fig. 5C) of each region at the thresholds of 0.15, 0.20, 0.25, and 0.27 were calculated and displayed in Fig. 5C. Both node degree and strength were greatly dependent on the threshold. Overall, ACC, S2, PF, Pari, 3a/3b, and pIns exhibited both high node degree and strengths at different thresholds. To decompose the overall graph (threshold of r at 0.15), fifteen broken-down graphs based on any two sub-networks are illustrated in Fig. 5D. There was no connection between subcortical and cortical sub-networks, except sub-network 1 and sub-network 3. The connector hub between

sub-networks 1 & 6, and 3 & 6 was MD; between sub-networks 2 & 3 and 3 & 5 were S2; between sub-networks 1 & 3, and 3 & 4 were pIns; between sub-networks 1 & 4 was ACC; between sub-networks 1 & 2 was Pari; between 2 & 4 was 7b; and between sub-networks 1 & 5, 2 & 5, 4 & 5 was area 3a/3b. The schematic of the relationships among the six pain sub-networks is summarized in Fig. 5E. Interestingly, from the more simplified graph (threshold of r at 0.27, Fig. 5F), we found that sub-network 2 (S2-pIns) connected sub-networks 1 (ACC-PF) and 5 (areas l/2–3a/3b). Generally, the MD thalamic nucleus served as a hub to connect subcortical and cortical pain sub-networks, and sensory and affective sub-networks are joined by the S2-pIns connection.

3.5. Hubs interconnect nociceptive sub-networks

Sub-network features identified by clustering and graph theory analyses are in good agreement. The unique dynamic FC (DFC) feature within each sub-network further supports the existence and parcellation of six nociceptive sub-networks: early sensory (area 3a/b and 1/2), high order sensory (S2 and pIns), associative sensory (area 7b and parietal area), anterior insula, cognitive/affective (PF and ACC), and subcortical (thalamic MD and VPL nuclei and caudate) networks (Fig. 6). Area 3a/3b, S2, pIns, parietal cortex, ACC, and MD are hubs that interconnect them. While cortical sub-networks are more interconnected, the sub-cortical network is more isolated. MD serves as the hub that connects cortical and sub-cortical sub-networks via ACC and pIns.

4. Discussion

4.1. Hierarchically organized nociceptive regions and networks in the primate brain

A hierarchically organized sensory nervous system, such as visual, auditory and touch, permits more efficient processing and integration of functionally specific input and information. In primates, a serial sensory information processing scheme has evolved to permit integration and modulation within and across sensory modalities (Kaas, 2004; Kaas and Collins, 2001, 2003). Apart from the well-characterized supraspinal tactile information processing pathways from the thalamic VP nucleus to areas 3b/1 of S1, S2 and PV (parietal ventral, subregions of S2 cortex) and posterior insula cortices, nociceptive information processing pathways around the central and lateral sulci and beyond have not been well-established and are under hot debate, mainly due to the lack of mechanistic characterization of nociceptive neurons and their functional connections in the primate brain. The primate brain is unique concerning the evolution of multiple distinct brain regions for nociceptive processing (e.g., areas 3a/3b/1/2 of S1, PV/S2, and area 7b) that are not readily discriminative in rodents (Kaas, 2004). While the roles of S1 and S2 cortices in the presentation of sensory aspects of painful information is well recognized and supported, emerging human functional neuroimaging and limited electrophysiological evidence from non-human primates have led to the hypothesis that the posterior insula may serve as the first (or primary) or important nociceptive-specific processing region (Garcia-Larrea et al., 2010; Iannetti et al., 2005; Segerdahl et al., 2015), even though the precise roles of this and other nociceptive regions remain to be established with gold-standard electrophysiological characterization of neuronal activity (Davis, 2003). Here our submillimeter resolution fMRI studies under light anesthesia have uncovered a more complex and refined thermal pain

networks that include S1 sub-regions, area 7b, dorsal parietal cortex, ACC, anterior and posterior insula, and frontal cortices for nociception in the primate brain. These brain regions activated by nociceptive heat stimulation under anesthesia without consciousness in monkeys were also activated in awake humans when thermal pain is perceived (Wager et al., 2013), indicating that these brain regions play a fundamental role in nociception. Future targeted electrophysiological investigations will need to be performed to fully understand the information processing and integration mechanisms that occur at each of these regions. One important note is that our recent combined high-resolution fMRI and electrophysiology studies have identified thermal nociceptive modality-specific (heat or cold nociceptive) modules and their own fine-scale distinct functional networks within the S1 cortex in its sub-regions (Yang et al., 2018). This particular study provided first-time evidence that not only supported the notion of separate nociceptive modality-specific processing pathways in the cortex but also validated the neuronal basis of nociception related fMRI signal changes and the use of fMRI for probing nociceptive networks in monkeys.

4.2. S2-pIns as a key hub in primate nociceptive system

One step further, in this present study, network analysis using either the functionally defined nociceptive regions as seeds or hypothesis-free data-driven graph theory methods, we successfully parcellated six nociception related cortical and subcortical sub-networks and identified the S2-pIns region as a key hub that interconnects sensory to affective (ACC) and cognitive (PF) regions networks. Our network hierarchical analysis identified S2-pIns region as a key hub that connects sensory nociceptive to emotional (ACC) and cognitive (PF) networks. S2 primarily connects to sensory S1 regions (areas 3a, 3b, 1 and 2) and area 7b, while pIns connect to affective ACC regions (Wu et al., 2017). These networks, interestingly, exhibited limited overlap. Graded fMRI and sensory evoked potentials were recorded in this region in monkeys. Existing anatomical connectivity evidence in this region in monkeys supports our functional observations of distinct function connectivity networks of these two regions (Coq et al., 2004; Neal et al., 1990; Nieuwenhuys, 2012). Functional connection between pIns and cingulate cortex (including ACC) (Raison, 2015) was also reported in the human brain (Taylor et al., 2009). These two regions in general are not readily distinguishable in human brain fMRI studies because of their close spatial proximity and limited spatial precision of localizing pain related fMRI activation (Iannetti et al., 2005), but there were studies showing distinct functional connections networks of insula sub-regions (Deen et al., 2011), a finding that is similar to our observations reported here. For a review of insula function in pain see (Isnard et al., 2011). Supporting their critical role in pain perception, focal lesions in both the homologous S2 and posterior insula in humans all resulted in changes in pain perception (Veldhuijzen et al., 2010). Taken together, these observations led us to hypothesize that S2-pIns may serve as a gate that controls or modulates the direction of sensory information flow to the next step in processing and integration. This hypothesis needs further investigation.

Together, these findings are significant because these various brain regions we detected under anesthesia in monkeys are known to be engaged in human pain perception. Nociceptive responses detected without consciousness in these high-order affective and cognitive regions underscore the fundamental role of the whole brain networks in processing

and integrating nociceptive inputs. Future mechanistic studies from neuronal activity perspectives will provide novel insights as to how different types of nociceptive inputs are processed and integrated locally and between regions or circuits (e.g., between S2-pIns to PF). To date, existing evidence from our group support the use of rsfMRI in delineating brain circuits and demonstrated the neuronal basis of nociceptive stimulation evoked fMRI signal changes and correlated fluctuation of resting state signals between cortical regions (Shi et al., 2017; Wang et al., 2013; Wilson et al., 2016; Yang et al., 2018).

4.3. Subcortical nociceptive networks and their distinct temporal dynamic connectivity features

The critical roles played by subcortical regions in pain perception and modulation have attracted more attention in recent years, particularly under chronic pain states. Some subcortical regions have been indicated in the pain processing and modulation, including the two thalamic and caudate nuclei we identified in our study (Emmert et al., 2014; Oshiro et al., 2007; Seixas et al., 2016). For example, pain associated putamen activity and connections have been reported in health subject's brain (Mhuircheartaigh et al., 2010), abnormalities were observed in chronic pain patients (Maleki et al., 2011; Scott et al., 2006). Pain-avoidance neurons, as well as thermal nociceptive neurons, were isolated in the caudate nucleus of awake macaques (Koyama et al., 2000). Similarly, with the use of a high signal-to-noise ratio provided by a high-field MRI and a customized whole brain volume coil, we showed here detection of nociceptive stimulus related fMRI activation in three subcortical regions (bilateral VPL and MD of the thalamus and caudate) under anesthesia which is known to reduce BOLD activities in both responses to inputs and at resting state (Mhuircheartaigh et al., 2010). The location of VPL activations appears to cover the territory of the posterior ventral medial nucleus (VMpo) region reported by Craig et al. (1994), but further work in the squirrel monkey is required to delineate the primate-specific VMpo relay. An important finding is that these three nuclei formed their own separate subcortical nociceptive network with distinct organizational features. The connectivity strength between MD and Cau appeared to be stronger than that between the two thalamic nuclei (MD-VPL) (Fig. 5B). Interestingly, graph theory analysis suggests that the MD thalamic nucleus serves as a hub that connects subcortical networks to cortical networks via the ACC and posterior insula region (Fig. 5A and E). Indeed, a previous anatomical tracer-tracking study revealed a direct monosynaptic connection between MD and ACC (Goldman-Rakic and Porrino, 1985; Vogt et al., 1987), and between MD-pIns in the monkey brain, even though the anterior insula appears to have a more extensive relationship with MD nuclei (Mufson and Mesulam, 1984). Compared to cortical networks, both nociceptive-stimulus evoked fMRI response and inter-regional functional connectivity were weaker in the sub-cortical network. We speculate that at least three factors, the relatively small size of these sub-cortical regions, which introduces a relatively high degree of partial volume effect, the degree of functional heterogeneity of their composition neurons, and anesthesia may contribute to the weaker nociceptive stimulus evoked response and inter-regional connectivity (Wu et al., 2016). We have shown previously that the functional similarity of composition neurons contributes greatly to the strengths of the synchrony of resting state signal fluctuation, a measure of functional connectivity (Wang et al., 2013).

Abnormal brain network dynamic has repeatedly been observed in chronic pain states (Baliki et al., 2008; Kucyi and Davis, 2015; Wang et al., 2017). The observation of distinct dynamic connectivity features exhibited by each of the six nociceptive sub-networks supports that dynamic feature of rsfMRI signal reflects independent functionality of each sub-networks. It could be used as a biomarker of functional integrity of subnetwork. Changes in temporal dynamics could be a sensitive indicator of the functional state of particular functional networks, such as pain networks. Our previous work supports this notion (Shi et al., 2016). We identified signatural temporal dynamics of rsFC in multiple functional networks including the mesoscale networks within S1 cortex in monkeys. It is commonly accepted that brain regions that belong to the same network tend to fluctuate with similar temporal dynamic features. For example, others' and our observations in chronic headache patients suggest that the network dynamic represents a functional feature of a tightly inter-connected networks (Baliki et al., 2008; Farmer et al., 2012; Wang et al., 2017), for a review see Kucyi and Davis (2015). Using the same dynamic measure, we found that in chronic headache patients, networks that exhibited weakened functional connections also showed less-variable (locked) temporal dynamics (Wang et al., 2017). Our data from this and previous studies further underscore the importance and potential clinical utility of temporal dynamic features in pain-related networks.

4.4. Whether the connection of the sub-networks reflects their anatomical proximity?

The close spatial proximity may have contributed to the strong connection, but we do not think it is the main driver for the following reasons. First, we observed high rsFC between two long-distance regions, such as between ACC and Pari bilateral. Second, our previous rsfMRI studies of local meso-scale cortical networks have demonstrated that the strength of the inter-regional rsFC is determined primarily by their functional similarity, not their spatial proximity. For example, our previous resting-state fMRI study of S1 sub-regions has shown that the rsFC strengths between digit regions in area 3b and area 1 were comparable to those between area 3a and area 1 (Wang et al., 2013). However, the cortical anatomical distance between distal finger pads (the skin site being stimulated in our study) representations in area 3a and area 1 is about two times larger than the distance between distal pads in areas 3b and 1. We think the strengths of the direct monosynaptic connections between brain regions are a main contributor to the rsFC strength. We believe that strong interconnections between a node's left and right hemisphere counterparts are reflective of their strong anatomical connection and functional similarity resulting from coordinated bilateral upper arm activity in the primates' daily life. This speculation is supported by our previous observations within areas 3b and 1 of S1 cortex in primates, where strong fingertip to tip rsFC corresponds to extensive anatomical connections (Shi et al., 2017; Wang et al., 2013).

A final note is that the parcellation of sub-networks is not as clearcut because it is influenced by the strengths of the connection and differences in the connection strengths and the nature of the parcellation methods. Because of this concern, we provided dynamic connectivity measures with different sliding windows (Fig. 4) and graph theory-defined networks using different thresholds (Fig. 5). Regardless of the thresholds chosen, a general pattern remains.

5. Conclusions

We observed six nociceptive subnetworks in NHP brain and each exhibited distinct dynamic connectivity features. S2-pIns and thalamic MD nucleus serve as two key hubs that interconnect sensorimotor and affective and cortical and subcortical networks. This work sets the stage for future direct stimulation studies that will determine the casual connection and information flow between different nociceptive sub-networks.

Supplementary Material

Refer to Web version on PubMed Central for supplementary material.

Acknowledgments

This study is supported by National Institutes of Health Grant R01 NS069909 to LMC and NS NS078680 to JCG. Dr. Wu is currently supported by NSFC (31700902 and 31871085), and Shanghai Municipal of Science and Technology Project (21ZR1407300 and 20JC1419500). We thank Chaohui Tang for her technical support on animal preparation, Fuxue Xin for his assistance on fMRI data collection, and Dr. Nellie Byun for language editing and Dr. Jamie Reed for proof-reading of the manuscript.

References

Apkarian AV, Baliki MN, Farmer MA, 2013. Predicting transition to chronic pain. Curr. Opin. Neurol. 26, 360–367. [PubMed: 23823463]

Apkarian AV, Bushnell MC, Treede RD, Zubieta JK, 2005. Human brain mechanisms of pain perception and regulation in health and disease. Eur. J. Pain 9, 463–484. [PubMed: 15979027]

Baliki MN, Geha PY, Apkarian AV, Chialvo DR, 2008. Beyond feeling: chronic pain hurts the brain, disrupting the default-mode network dynamics. J. Neurosci. 28, 1398–1403. [PubMed: 18256259]

Chen LM, Dillenburger BC, Wang F, Friedman RM, Avison MJ, 2011. High-resolution functional magnetic resonance imaging mapping of noxious heat and tactile activations along the central sulcus in new world monkeys. Pain 152, 522–532. [PubMed: 21177033]

Chen LM, Dillenburger BC, Wang F, Tang CH, 2012. Differential fMRI activation to noxious heat and tactile stimuli in parasylvian areas of new world monkeys. Pain 153, 158–169. [PubMed: 22115923]

Chen LM, Yang PF, Wang F, Mishra A, Shi Z, Wu R, Wu TL, Wilson GH, Ding Z, Gore JC, 2017. Biophysical and neural basis of resting state functional connectivity: evidence from non-human primates. Magn. Reson. Imaging 39, 71–81. [PubMed: 28161319]

Coq JO, Qi H, Collins CE, Kaas JH, 2004. Anatomical and functional organization of somatosensory areas of the lateral fissure of the new world titi monkey (Callicebus moloch). J. Comp. Neurol. 476, 363–387. [PubMed: 15282711]

Craig AD, Bushnell MC, Zhang ET, Blomqvist A, 1994. A thalamic nucleus specific for pain and temperature sensation. Nature 372, 770–773. [PubMed: 7695716]

Davis KD, 2003. Neurophysiological and anatomical considerations in functional imaging of pain. Pain 105, 1–3. [PubMed: 14499413]

Deen B, Pitskel NB, Pelphrey KA, 2011. Three systems of insular functional connectivity identified with cluster analysis. Cereb. Cortex 21, 1498–1506. [PubMed: 21097516]

Edelbrock C, McLaughlin B, 1980. Hierarchical cluster analysis using intraclass correlations: a mixture model study. Multivar. Behav. Res. 15, 299–318.

Emmert K, Breimhorst M, Bauermann T, Birklein F, Van De Ville D, Haller S, 2014. Comparison of anterior cingulate vs. insular cortex as targets for real-time fMRI regulation during pain stimulation. Front. Behav. Neurosci. 8, 350. [PubMed: 25346666]

Farmer MA, Baliki MN, Apkarian AV, 2012. A dynamic network perspective of chronic pain. Neurosci. Lett. 520, 197–203. [PubMed: 22579823]

Fornito A, Zalesky A, Bullmore ET, 2010. Network scaling effects in graph analytic studies of human resting-state FMRI data. Front. Syst. Neurosci. 4, 22. [PubMed: 20592949]

Garcia-Larrea L, Perchet C, Creac'h C, Convers P, Peyron R, Laurent B, Mauguiere F, Magnin M, 2010. Operculo-insular pain (parasylvian pain): a distinct central pain syndrome. Brain 133, 2528–2539. [PubMed: 20724291]

Gergen JA, MacLean PD, 1962. A stereotaxic atlas of the squirrel monkey's brain (saimiri sciureus). Public Health Serv. Publ. No. 933.

Gerits A, Farivar R, Rosen BR, Wald LL, Boyden ES, Vanduffel W, 2012. Optogenetically induced behavioral and functional network changes in primates. Curr. Biol. 22, 1722–1726. [PubMed: 22840516]

Glover GH, Li TQ, Ress D, 2000. Image-based method for retrospective correction of physiological motion effects in fMRI: RETROICOR. Magn. Reson. Med. 44, 162–167. [PubMed: 10893535]

Goldman-Rakic PS, Porrino LJ, 1985. The primate mediodorsal (MD) nucleus and its projection to the frontal lobe. J. Comp. Neurol. 242, 535–560. [PubMed: 2418080]

Gorsuch RL, Lehmann CS, 2010. Correlation coefficients: mean bias and confidence interval distortions. JMM 1, 52–65.

Hutchison RM, Womelsdorf T, Allen EA, Bandettini PA, Calhoun VD, Corbetta M, Della Penna S, Duyn JH, Glover GH, Gonzalez-Castillo J, Handwerker DA, Keilholz S, Kiviniemi V, Leopold DA, de Pasquale F, Sporns O, Walter M, Chang C, 2013a. Dynamic functional connectivity: promise, issues, and interpretations. Neuroimage 80, 360–378. [PubMed: 23707587]

Hutchison RM, Womelsdorf T, Gati JS, Everling S, Menon RS, 2013b. Resting-state networks show dynamic functional connectivity in awake humans and anesthetized macaques. Hum. Brain Mapp. 34, 2154–2177. [PubMed: 22438275]

Iannetti GD, Zambreanu L, Cruccu G, Tracey I, 2005. Operculoinsular cortex encodes pain intensity at the earliest stages of cortical processing as indicated by amplitude of laser-evoked potentials in humans. Neuroscience 131, 199–208. [PubMed: 15680703]

Isnard J, Magnin M, Jung J, Mauguiere F, Garcia-Larrea L, 2011. Does the insula tell our brain that we are in pain? Pain 152, 946–951. [PubMed: 21277680]

Johnson SC, 1967. Hierarchical clustering schemes. Psychometrika 32, 241–254. [PubMed: 5234703]

Jones EG, Burton H, 1976. Areal differences in the laminar distribution of thalamic afferents in cortical fields of the insular, parietal and temporal regions of primates. J. Comp. Neurol. 168, 197–247. [PubMed: 821974]

Kaas JH, 2004. Evolution of somatosensory and motor cortex in primates. Anat. Rec. A Discov. Mol. Cell Evol. Biol. 281, 1148–1156. [PubMed: 15470673]

Kaas JH, Collins CE, 2001. The organization of sensory cortex. Curr. Opin. Neurobiol. 11, 498–504. [PubMed: 11502398]

Kaas JH, Collins CE, 2003. The organization of somatosensory cortex in anthropoid primates. Adv. Neurol. 93, 57–67. [PubMed: 12894401]

Kim JH, Choi SH, Jang JH, Lee DH, Lee KJ, Lee WJ, Moon JY, Kim YC, Kang DH, 2017. Impaired insula functional connectivity associated with persistent pain perception in patients with complex regional pain syndrome. PLoS One 12, e0180479. [PubMed: 28692702]

Klink PC, Aubry JF, Ferrera VP, Fox AS, Froudist-Walsh S, Jarraya B, Konofagou EE, Krauzlis RJ, Messinger A, Mitchell AS, Ortiz-Rios M, Oya H, Roberts AC, Roe AW, Rushworth MFS, Sallet J, Schmid MC, Schroeder CE, Tasserie J, Tsao DY, Uhrig L, Vanduffel W, Wilke M, Kagan I, Petkov CI, 2021. Combining brain perturbation and neuroimaging in non-human primates. Neuroimage 235.

Koyama T, Kato K, Mikami A, 2000. During pain-avoidance neurons activated in the macaque anterior cingulate and caudate. Neurosci. Lett. 283, 17–20. [PubMed: 10729623]

Kucyi A, Davis KD, 2015. The dynamic pain connectome. Trends Neurosci. 38, 86–95. [PubMed: 25541287]

Kucyi A, Davis KD, 2017. The neural code for pain: from single-cell electrophysiology to the dynamic pain connectome. Neuroscientist 23, 397–414. [PubMed: 27660241]

Lv Q, Yang L, Li G, Wang Z, Shen Z, Yu W, Jiang Q, Hou B, Pu J, Hu H, Wang Z, 2016. Large-scale persistent network reconfiguration induced by ketamine in anesthetized monkeys: relevance to mood disorders. Biol. Psychiatry 79, 765–775. [PubMed: 25837427]

Maleki N, Becerra L, Nutile L, Pendse G, Brawn J, Bigal M, Burstein R, Borsook D, 2011. Migraine attacks the basal ganglia. Mol. Pain 7, 71. [PubMed: 21936901]

Mhuircheartaigh RN, Rosenorn-Lanng D, Wise R, Jbabdi S, Rogers R, Tracey I, 2010. Cortical and subcortical connectivity changes during decreasing levels of consciousness in humans: a functional magnetic resonance imaging study using propofol. J. Neurosci. 30, 9095–9102. [PubMed: 20610743]

Mrvar A, Batagelj V, 1998. Pajek-program for large network analysis. Connections 21, 47–57.

Mufson EJ, Mesulam MM, 1984. Thalamic connections of the insula in the rhesus monkey and comments on the paralimbic connectivity of the medial pulvinar nucleus. J. Comp. Neurol. 227, 109–120. [PubMed: 6470205]

Neal JW, Pearson RC, Powell TP, 1990. The ipsilateral cortico-cortical connections of area 7b, PF, in the parietal and temporal lobes of the monkey. Brain Res. 524, 119–132. [PubMed: 1698108]

Nieuwenhuys R, 2012. The insular cortex: a review. Evol. Primate Brain Neuron Behav. 195, 123–163.

Oshiro Y, Quevedo AS, McHaffie JG, Kraft RA, Coghill RC, 2007. Brain mechanisms supporting spatial discrimination of pain. J. Neurosci. 27, 3388–3394. [PubMed: 17392455]

Raison CL, 2015. Cingulate and insula: the pain in the brain is not all the same. Biol. Psychiatry 77, 205–206. [PubMed: 25542514]

Rubinov M, Sporns O, 2010. Complex network measures of brain connectivity: uses and interpretations. Neuroimage 52, 1059–1069. [PubMed: 19819337]

Sawamoto N, Honda M, Okada T, Hanakawa T, Kanda M, Fukuyama H, Konishi J, Shibasaki H, 2000. Expectation of pain enhances responses to nonpainful somatosensory stimulation in the anterior cingulate cortex and parietal operculum/posterior insula: an event-related functional magnetic resonance imaging study. J. Neurosci. 20, 7438–7445. [PubMed: 11007903]

Scott DJ, Heitzeg MM, Koeppe RA, Stohler CS, Zubieta JK, 2006. Variations in the human pain stress experience mediated by ventral and dorsal basal ganglia dopamine activity. J. Neurosci. 26, 10789–10795. [PubMed: 17050717]

Segerdahl AR, Mezue M, Okell TW, Farrar JT, Tracey I, 2015. The dorsal posterior insula subserves a fundamental role in human pain. Nat. Neurosci. 18, 499–500. [PubMed: 25751532]

Seixas D, Palace J, Tracey I, 2016. Chronic pain disrupts the reward circuitry in multiple sclerosis. Eur. J. Neurosci. 44, 1928–1934. [PubMed: 27178661]

Shi Z, Rogers BP, Chen LM, Morgan VL, Mishra A, Wilkes DM, Gore JC, 2016. Realistic models of apparent dynamic changes in resting-state connectivity in somatosensory cortex. Hum. Brain Mapp. 37, 3897–3910. [PubMed: 27296233]

Shi Z, Wu R, Yang PF, Wang F, Wu TL, Mishra A, Chen LM, Gore JC, 2017. High spatial correspondence at a columnar level between activation and resting state fMRI signals and local field potentials. Proc. Natl. Acad. Sci. U. S. A. 114, 5253–5258. [PubMed: 28461461]

Sokal RR, Michener DD, 1958. A statistical method for evaluating systematic relationships. Univ. Kansas Sci. Bull. 38, 1409–1438.

Taylor KS, Seminowicz DA, Davis KD, 2009. Two systems of resting state connectivity between the insula and cingulate cortex. Hum. Brain Mapp. 30, 2731–2745. [PubMed: 19072897]

Veldhuijzen DS, Greenspan JD, Kim JH, Lenz FA, 2010. Altered pain and thermal sensation in subjects with isolated parietal and insular cortical lesions. Eur. J. Pain 14 535 e531–511.

Vogt BA, Pandya DN, Rosene DL, 1987. Cingulate cortex of the rhesus monkey: I. Cytoarchitecture and thalamic afferents. J. Comp. Neurol. 262, 256–270. [PubMed: 3624554]

Wager TD, Atlas LY, Lindquist MA, Roy M, Woo CW, Kross E, 2013. An fMRI-based neurologic signature of physical pain. N. Engl. J. Med. 368, 1388–1397. [PubMed: 23574118]

Wang Z, Chen LM, Negyessy L, Friedman RM, Mishra A, Gore JC, Roe AW, 2013. The relationship of anatomical and functional connectivity to resting-state connectivity in primate somatosensory cortex. Neuron 78, 1116–1126. [PubMed: 23791200]

Wang Z, Yang Q, Chen LM, 2017. Abnormal dynamics of cortical resting state functional connectivity in chronic headache patients. Magn. Reson. Imaging 36, 56–67. [PubMed: 27751859]

Wilson GH, Yang PF, Gore JC, Chen LM, 2016. Correlated inter-regional variations in low frequency local field potentials and resting state BOLD signals within S1 cortex of monkeys. Hum. Brain Mapp. 37, 2755–2766. [PubMed: 27091582]

Wu R, Wang F, Yang PF, Chen LM, 2017. High-resolution functional MRI identified distinct global intrinsic functional networks of nociceptive posterior insula and S2 regions in squirrel monkey brain. Neuroimage 155, 147–158. [PubMed: 28461059]

Wu TL, Mishra A, Wang F, Yang PF, Gore JC, Chen LM, 2016. Effects of isoflurane anesthesia on resting-state fMRI signals and functional connectivity within primary somatosensory cortex of monkeys. Brain Behav. 6, e00591. [PubMed: 28032008]

Xu AG, Qian M, Tian F, Xu B, Friedman RM, Wang J, Song X, Sun Y, Chernov MM, Cayce JM, Jansen ED, Mahadevan-Jansen A, Zhang X, Chen G, Roe AW, 2019. Focal infrared neural stimulation with high-field functional MRI: a rapid way to map mesoscale brain connectomes. Sci. Adv. 5, eaau7046. [PubMed: 31032400]

Yang PF, Phipps MA, Jonathan S, Newton AT, Byun N, Gore JC, Grissom WA, Caskey CF, Chen LM, 2021. Bidirectional and state-dependent modulation of brain activity by transcranial focused ultrasound in non-human primates. Brain Stimul. 14, 261–272. [PubMed: 33460838]

Yang PF, Wu R, Wu TL, Shi Z, Chen LM, 2018. Discrete modules and mesoscale functional circuits for thermal nociception within primate S1 cortex. J. Neurosci. 38, 1774–1787. [PubMed: 29335352]

Ye X, Yang PF, Liu Q, Dillenburger BD, Friedman RM, Chen LM, 2021. A thermal nociceptive patch in the S2 cortex of nonhuman primates: a combined functional magnetic resonance imaging and electrophysiology study. Pain 162, 2705–2716. [PubMed: 33945242]

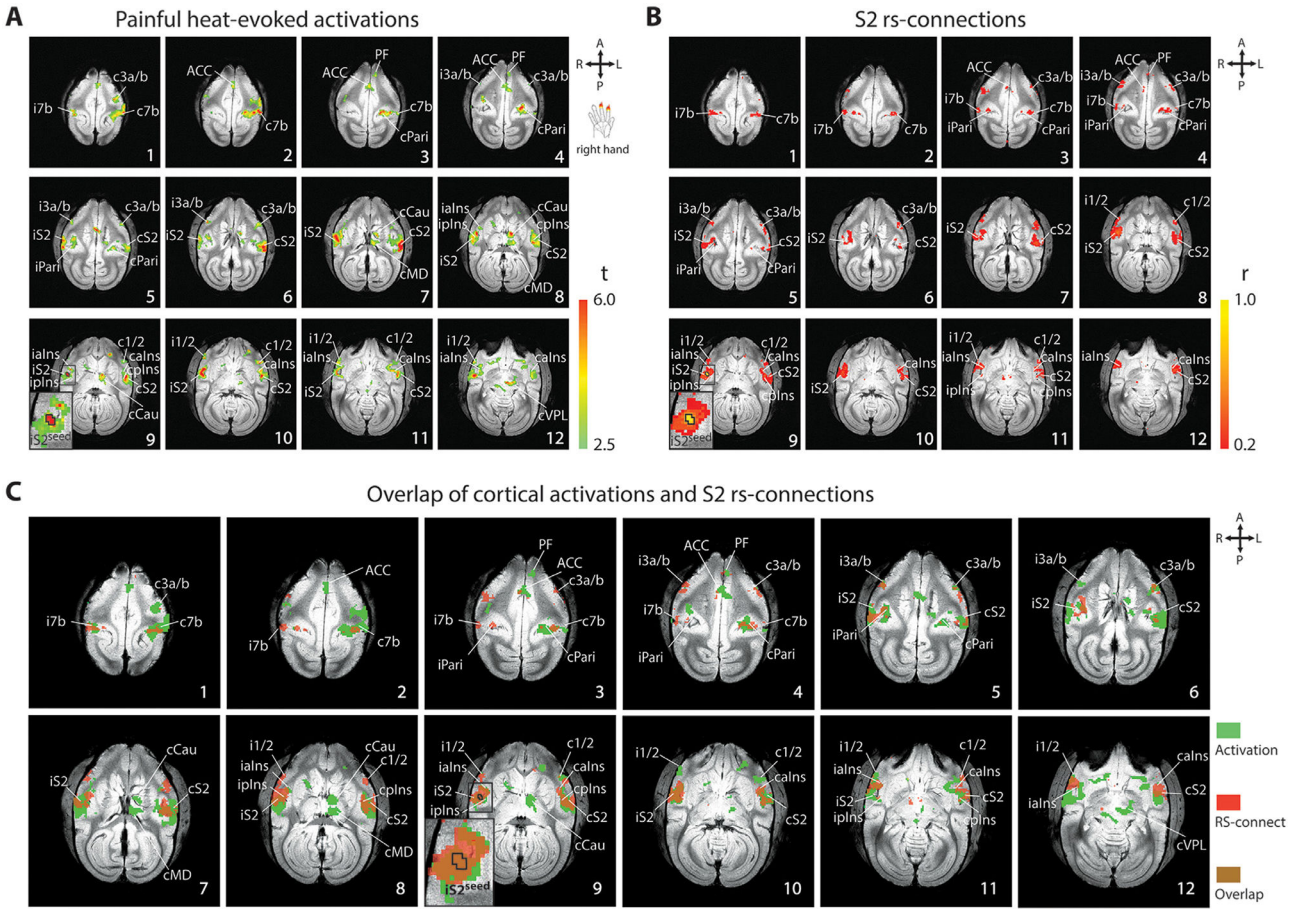

Fig. 1.

Similarity and spatial correspondence of nociceptive heat-evoked cortical fMRI activation and cortical nociceptive rsFC of ipsilateral S2 in one representative squirrel monkey (SM-H, session 1). (A) Axial images, sampled from top to bottom of the brain, show multi-run fMRI activation to simultaneous 47 °C heat stimulation of the right-hand D2 and D3 distal and middle phalanges (n = 12 runs). Color bar indicates the range of t-values. The S2 seed is outlined by black line on slice 9. Orientations (A: anterior, P: posterior, R: right, L: left) and slice numbers are marked on the images. (B) Multiple run averaged nociceptive iS2-seed based rsFC maps illustrate intrinsic connections of S2 seed among pain-related cortical regions (n = 4 runs). (C) Spatial composite maps (brown) of nociceptive cortical activation (green) and intrinsic functional connectivity maps of the S2 nociceptive region (red). Axial slices represented are 1 mm apart. ACC: anterior cingulate cortex; caIns: contralateral anterior insula; cCAU: contralateral caudate; cMD: contralateral mediodorsal thalamic nucleus; cPari: contralateral posterior parietal cortex; cpIns: contralateral posterior insula; cS2: contralateral secondary somatosensory cortex; cVPL: contralateral ventral posterolateral thalamic nucleus; c1/2: contralateral area 1/2; c3a/b: contralateral area 3a/3b; c7b: contralateral area 7b; iaIns: ipsilateral anterior insula; iPari: ipsilateral posterior parietal cortex; ipIns: ipsilateral posterior insula; iS2: ipsilateral secondary somatosensory cortex; $iS2^{seed}$: ipsilateral S2 seed; i1/2:ipsilateral area 1/2; i3a/b: ipsilateral area 3a/3b; i7b: ipsilateral area 7b; PF: prefrontal cortex.

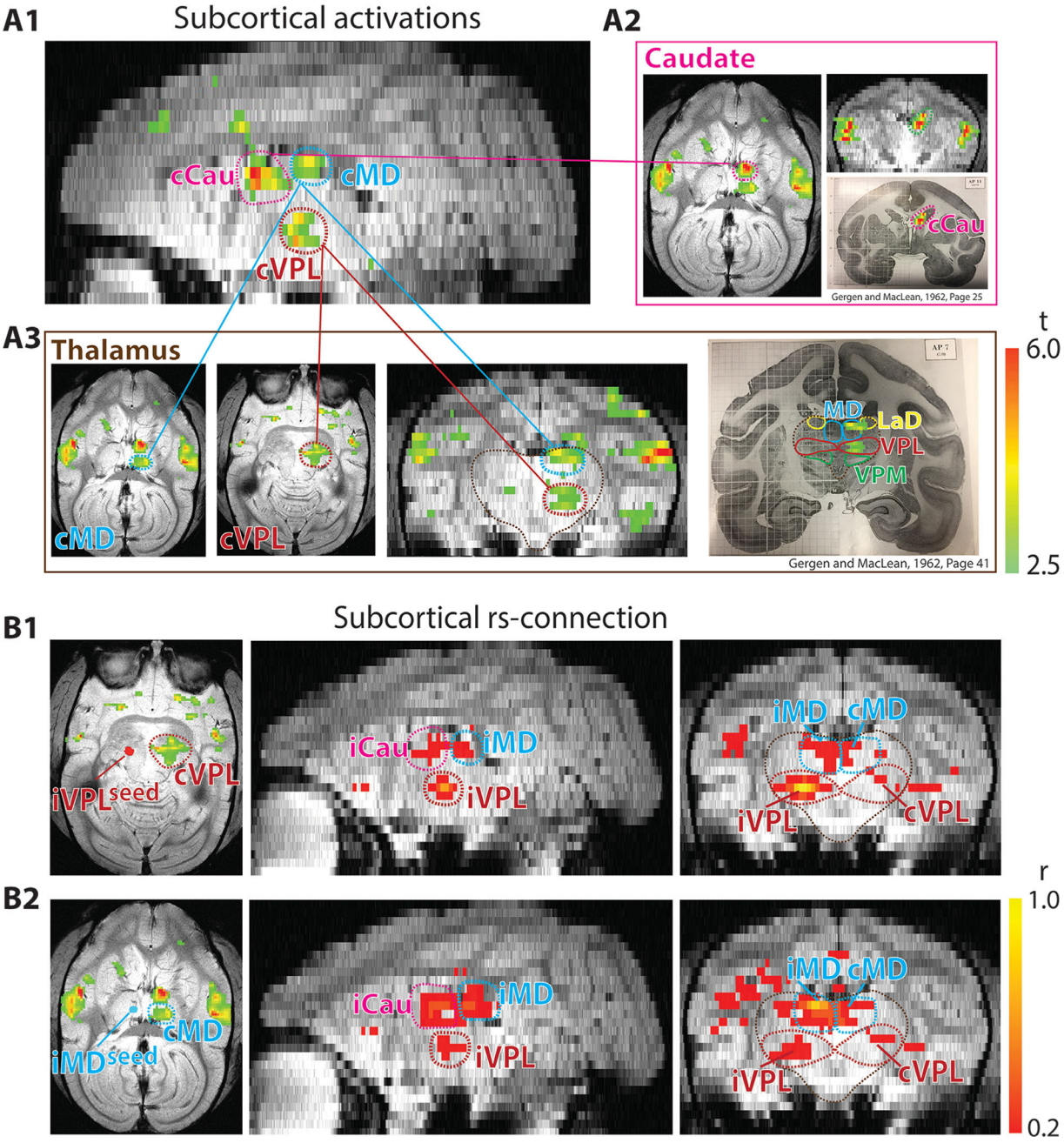

Fig. 2.

Comparison of nociceptive heat-evoked fMRI activation in subcortical regions and rsFC pattern of nociceptive thalamic nucleus. Results shown for the same representative session as Fig. 1 (session 1 of SM-H). (A1-A3) Heat-evoked subcortical activation maps in the reconstructed (sagittal (A1), axial and coronal (A2-A3) planes with the corresponding squirrel monkey atlas (Gergen and MacLean, 1962, pages 25 and 41) show the subcortical activation locations in caudate (Cau) nucleus (A2) and medial dorsal (MD) and ventral posterolateral (VPL) thalamic nuclei (A3). (B1-B2) Multi-run nociceptive ipsilateral VPL-

seed (B1) and ipsilateral MD-seed based subcortical connections at rest in axial and coronal images. VPL and MD seeds are indicated on the heat maps (left of B1 and B2 respectively).

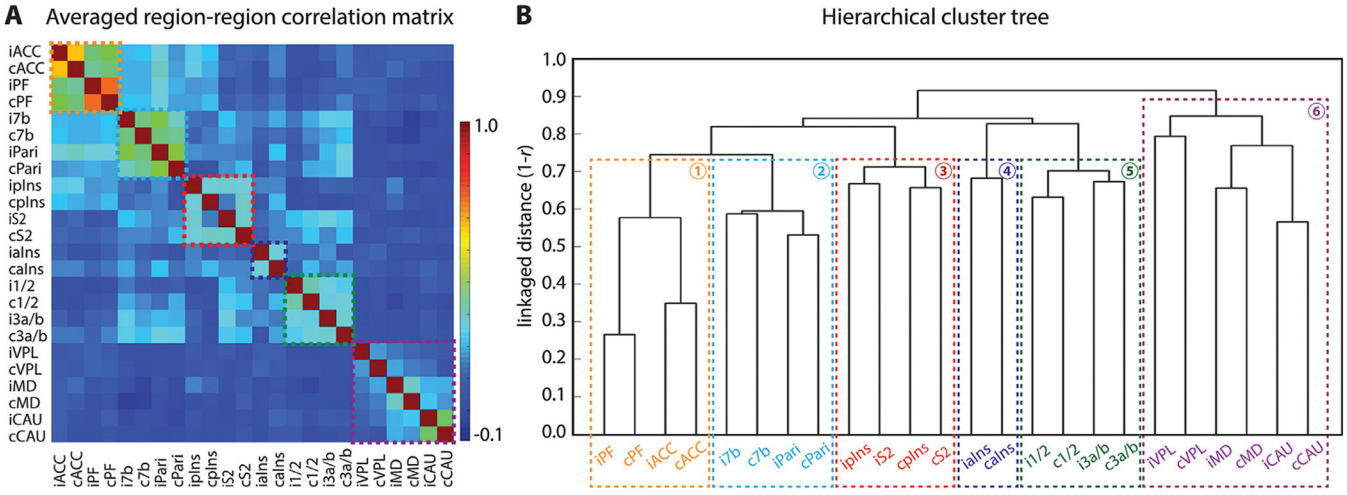

Fig. 3.

Functional connectivity relationships among the regions identified in nociceptive activation maps. (A) A 2D matrix plot of the group (n = 14 resting state runs, 4 sessions and 3 monkeys) averaged inter-regional correlation strength (r-value, see color bar for range). (B) Hierarchical cluster tree organization of connectivity strength rankings of all 24 seeds. Six sub-networks are parsed. The y-axis indicates the distance (1-r) used for clustering with a weighted average-linkage algorithm (WPGMA). A total of 14 resting-state fMRI runs from 4 sessions were included in the quantification.

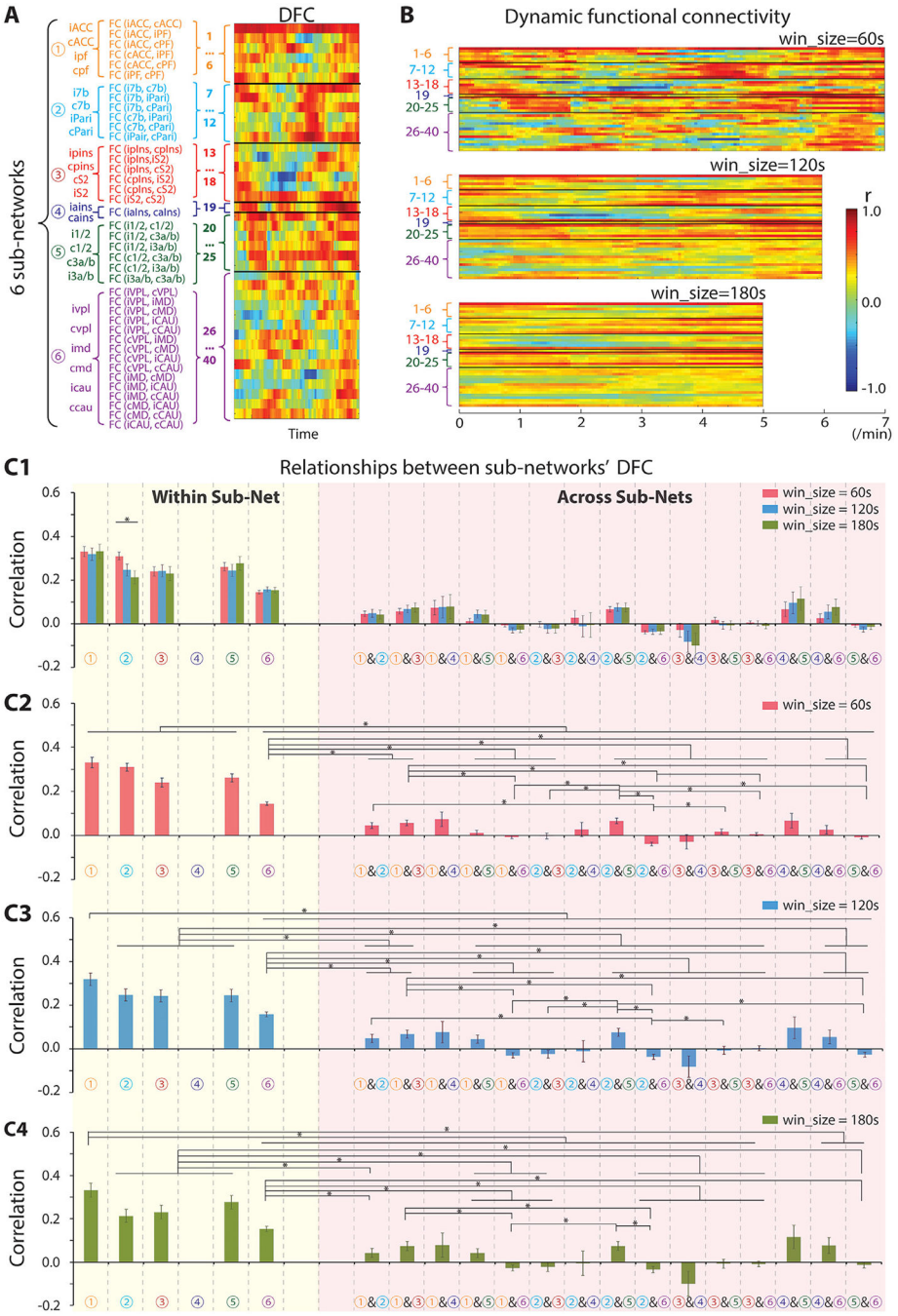

Fig. 4.

Temporal dynamic functional connectivity (DFC) features of six nociceptive sub-networks. (A) Scheme of DFC analysis across six sub-networks and a representative DFC example from one run of session 1 of SM-H. (B) Example of a DFC profile of the seed regions with sliding-window sizes of 60 s (top), 120 s (middle), and 180 s (bottom). (C1) DFC relationships within (yellow column) and across sub-networks (pink column). (C2-C4) DFC relationships within (yellow column) and across sub-networks (pink column) with sliding-window size of 60 s (C2), 120 s (C3), and 180 s (C4). The total number of DFC pairs within

sub-network 1, 2, 3, or 5 is 210, and that from 6 is 1470. The number of DFC pairs across sub-networks 1 & 2, 1 & 3, 1 & 5, 2 & 3, 2 & 5, or 3 & 5 is 504, across sub-network 1 & 4, 2 & 4, 3 & 4, or 4 & 5 is 84, across sub-network 1 & 6, 2 & 6, 3 & 6, or 5 & 6 is 1260, and across sub-network 4 & 6 is 210. Sidak's multiple comparisons test, $*p < 0.05$, Error bars indicate standard error.

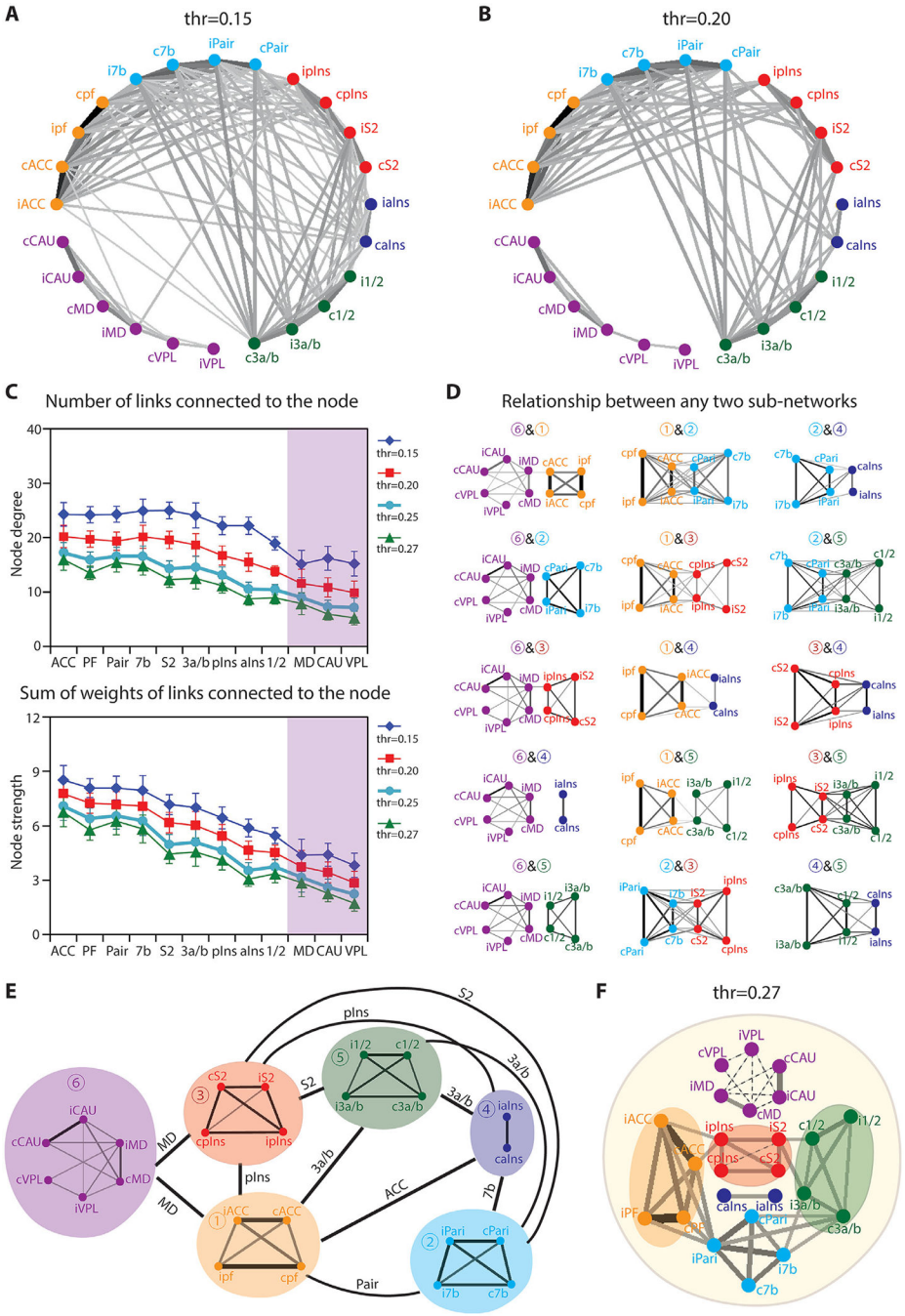

Fig. 5.

Graph theory analysis of global nociceptive networks. (A-B) Node-node connections of pain related-regions thresholded at $r = 0.15$ ($p < 0.05$, A) and $r = 0.20$ ($p < 0.01$, B). (C) Node degree (upper) and strength (lower) of pain related-regions at thresholds of $r = 0.15$ ($p < 0.05$, blue line), $r = 0.20$ ($p < 0.01$, red line), $r = 0.25$ ($p < 0.005$, cyan line), and $r = 0.27$ ($p < 0.001$, green line). (D) Plots of connectivity strengths between any pairs of sub-network at the threshold of $r = 0.15$ ($p < 0.05$). (E) Schematic summary of the relationships among the

six pain sub-networks. (F) Relationship among sub-networks at the threshold of $r = 0.27$ ($p < 0.001$).

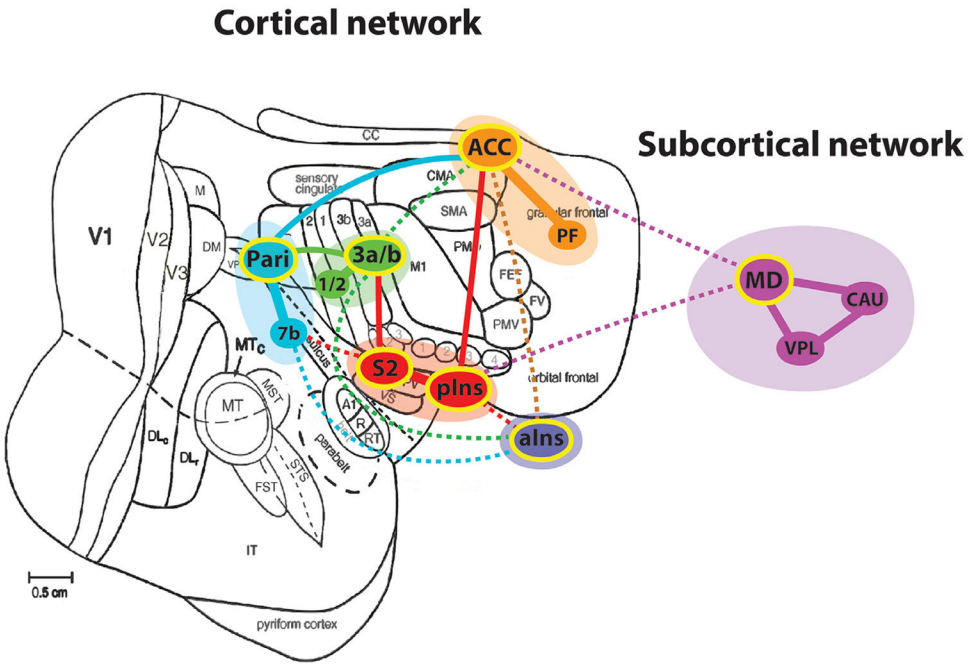

Fig. 6.

Schematic illustration of nociceptive networks identified in the squirrel monkey brain. Modified from Kaas and Collins (2001). Regions with yellow outline indicate the subnetwork hubs. Dotted lines indicate weaker connections. Each color represents one subnetwork. ACC: anterior cingulate cortex; aIns: anterior insula; CAU: caudate; MD: mediodorsal thalamic nucleus; Pari: posterior parietal cortex; PF: prefrontal cortex; pIns: posterior insula; S2: secondary somatosensory cortex; VPL: ventral posterolateral thalamic nucleus; 1/2: area 1/2; 3a/b: area 3a/3b; 7b: area 7b.